Table S1. Genetic mutation rates of core CDH genes based on targeted exon sequencing in melanoma samples from Taiwanese patients

Gene	Extracellular domain and transmembrane mutation rate (%)	Substitution events[a]	Intracellular domain mutation rate (%)	Substitution events[a]	Total mutation rate (%) (cases/ total samples)
CDH6	9.09%	exon9:c.A1400G:p.K467R	18.18%	exon12:c.G2170A:p.D724N exon12:c.G2236A:p.V746M	22.73% (5/22)
CDH10	18.18%	exon3:c.C346G:p.R116G exon3:c.C377T:p.T126I exon5:c.G607A:p.E203K exon7:c.C1163T:p.S388F	9.09%	exon12:c.G2044A:p.E682K	22.73% (5/22)
CDH18	13.63%	exon4:c.G310A:p.D104N exon8:c.G1124A:p.G375E exon9:c.G455A:p.G152E	13.63%	exon16:c.G2345A:p.G782E	22.73% (5/22)
CDH12	18.18%	exon6:c.C28T:p.L10F exon6:c.C65T:p.P22L exon12:c.T1301C:p.I434T exon15:c.G1802A:p.C601Y exon16:c.C2186T:p.T729I	0%	None detected	18.18% (4/22)
CDH9	9.09%	exon2:c.C62T:p.T21I exon4:c.G541A:p.V181I	0%	None Detected	13.63% (3/22)
CDH24	9.09%	exon3:c.C395T:p.P132L exon3:c.C470T:p.A157V	4.54%	exon13:c.G2036A:p.R679Q	13.63% (3/22)

		exon8:c.G1279A:p.E427K			
CDH1	9.09%	exon8:c.C1082T:p.A361V exon10:c.G1483A:p.V495M	4.54	exon14:c.G2287A:p.E763K	9.09% (2/22)
CDH2	4.54%	exon9:c.G1276A:p.D426N exon11:c.C1725A:p.F575L	9.09%	exon15:c.G2476A:p.A826T exon16:c.T2593G:p.S865A	9.09% (2/22)
CDH4	9.09%	exon1:c.C44T:p.P15L exon14:c.A2338C:p.I780L	0%	None detected	9.09% (2/22)
CDH5	9.09%	exon4:c.C556T:p.H186Y exon11:c.G1798A:p.A600T	0%	None detected	9.09% (2/22)
CDH7	9.09%	exon3:c.G433A:p.D145N exon11:c.G1789A:p.E597K exon11:c.G1864A:p.V622M	4.54%	exon12:c.C2264T:p.S755F	9.09% (2/22)
CDH8	9.09%	exon3:c.G340A:p.V114I exon3:c.C445G:p.P149A exon10:c.A1589C:p.Y530S	0%	None detected	9.09% (2/22)
CDH11	9.09%	exon3:c.C65T:p.A22V exon5:c.G607A:p.E203K	0%	None detected	9.09% (2/22)
CDH13	4.54%	exon5:c.C557T:p.S186F exon6:c.G760A:p.V254I	9.09%	exon14:c.C2143T:p.P715S exon14:c.G2170A:p.V724I	9.09% (2/22)
CDH15	4.54%	exon9:c.G1306A:p.V436M	0%	Not detected	4.54% (1/22)

[a]c- chromosomal base substitution; p- amino acid substitution

Table S2. Calculation of catenin-binding free energy differences between WT and known mutations in core CDH genes in melanoma

Mutation	Protein	Domain	Binding protein	$\Delta\Delta G_{Binding}^{Mutation}$ (kJ/mol)
D661N	CDH6, CDH9, CDH10	JMD	p120-catenin	4.60 ± 0.69
E662K	CDH6, CDH9	JMD	p120-catenin	7.50 ± 2.11
G663E	CDH18	JMD	p120-catenin	42.29 ± 7.57
G665R	CDH10	JMD	p120-catenin	-15.34 ± 13.85
E666K	CDH9	JMD	p120-catenin	21.95 ± 4.39
E667K	CDH18	JMD	p120-catenin	1.56 ± 2.88
R689Q	CDH6	CBD	β-catenin	8.17 ± 4.91
D691N	CDH6	CBD	β-catenin	5.96 ± 0.96
E722K	CDH6	CBD	β-catenin	-0.07 ± 5.04
D726N	CDH6	CBD	β-catenin	5.98 ± 1.77
D733N	CDH9	CBD	β-catenin	15.62 ± 1.83
E741K	CDH9	CBD	β-catenin	16.38 ± 2.35
G742E	CDH10	CBD	β-catenin	-19.63 ± 6.25
L767F	CDH10	CBD	β-catenin	-1.60 ± 5.56
R773Q	CDH6, CDH9	CBD	β-catenin	8.70 ± 5.05

Table S3. Gene set enrichment analyses of reactomes/pathways concurrently up-regulated with mutations in top-four core CDH genes in melanoma[a]

Reactome /Pathway[b]	ES	NES	NOM p-value
1. Liver_Cancer_Subclass_G3_Up	0.6493	1.7587	0.0159
2. Doxorubicin_Resistance_Up	0.7836	1.6533	0.0175
3. Antigen_Response	0.6726	1.7603	0.0236
4. Thyroid_Carcinoma_Anaplastic_Up	0.5938	1.7737	0.0276
5. T_Lymphocyte_Up	0.7554	1.6582	0.0320
6. Epithelial_Mesenchymal_Transition_Up	0.6731	1.7110	0.0333
7. M_G1_Transition	0.6640	1.6491	0.0345
8. Core_Serum_Response_Up	0.6037	1.6801	0.0352
9. Cell_Cycle_Mitotic	0.6362	1.6307	0.0369
10. Synthesis_Of_DNA	0.6648	1.6498	0.0381
11. Mitotic_G1/G1_S_Phases	0.5985	1.6321	0.0386
12. CDC20_Mediated_Degradation_Of_Mitotic_Proteins	0.6666	1.6343	0.0423
13. DNA_Replication	0.6606	1.6724	0.0437
14. Mitotic_M/M_G1_Phases	0.6589	1.6693	0.0437
15. Cervical_Cancer_Proliferation_Cluster	0.6992	1.6660	0.0483

[a]Abbreviations: ES, enrichment score; NES, normalized enrichment score; NOM p-value, nominalized p-value.

[b]Reactomes or pathways with NOM p-values < 0.05 were considered as significantly relevant with mutations in top-four core CDH genes.
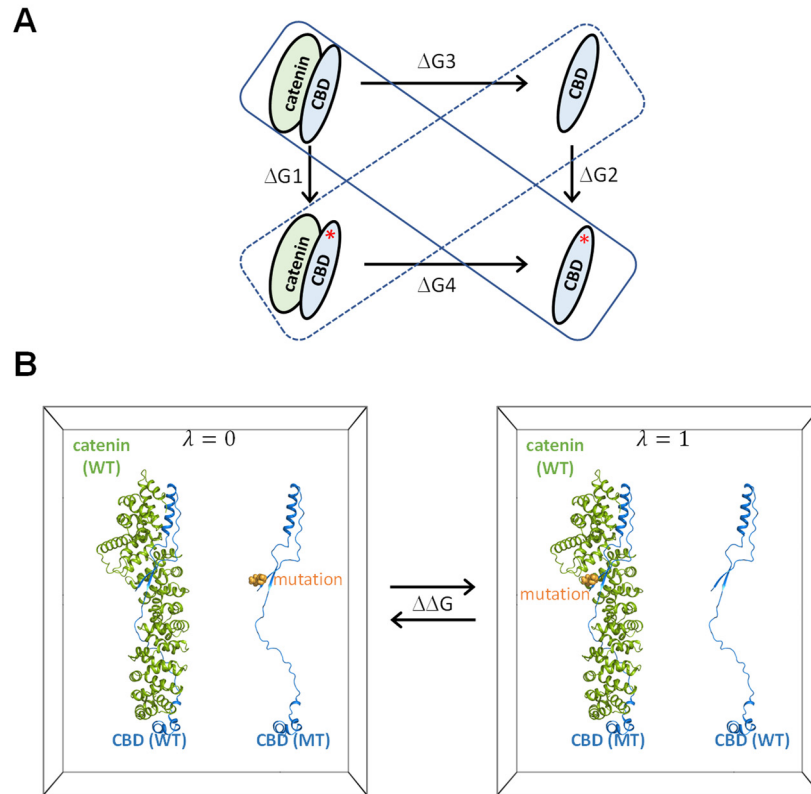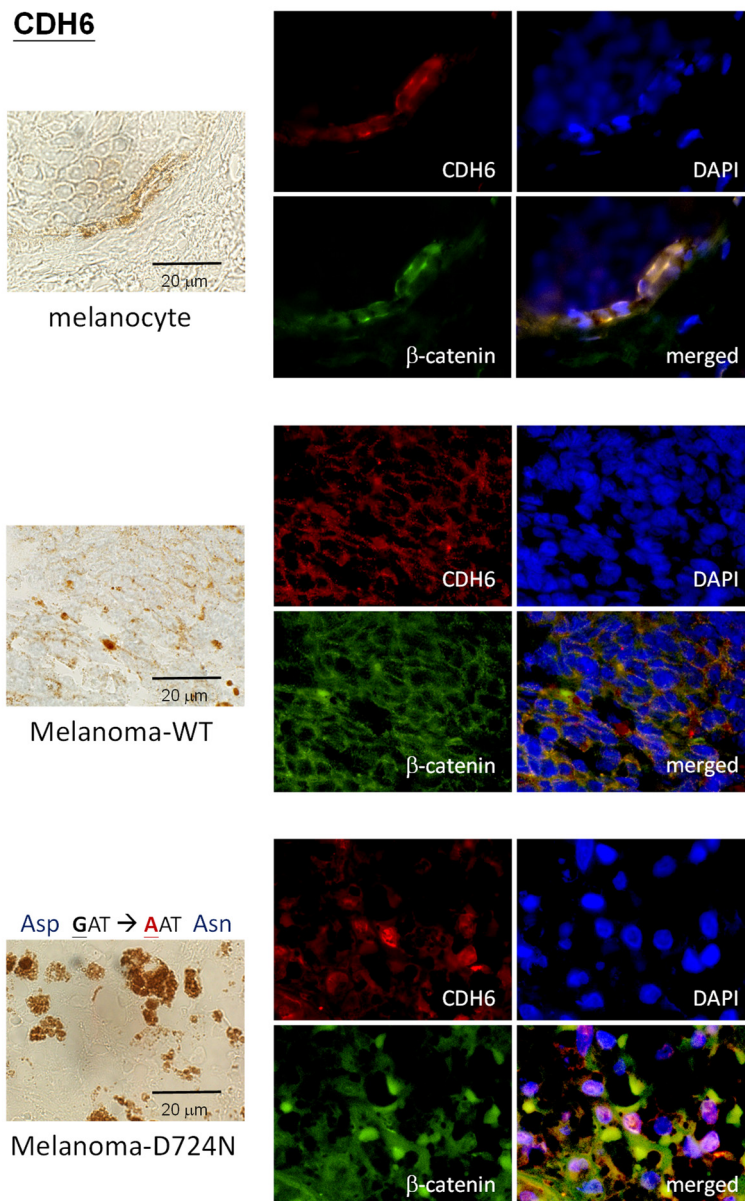
Figure S1. Double-system/single-box setup. (A) Two branches of a thermodynamic cycle are placed in one simulation box. The different boxes in the scheme are indicated by the solid ($\lambda = 0$) and broken ($\lambda = 1$) lines. (B) An example of a simulation setup for the catenin binding free energy calculation. The free energy difference corresponds to a double free energy difference: $\Delta\Delta G = \Delta G1 - \Delta G2$.
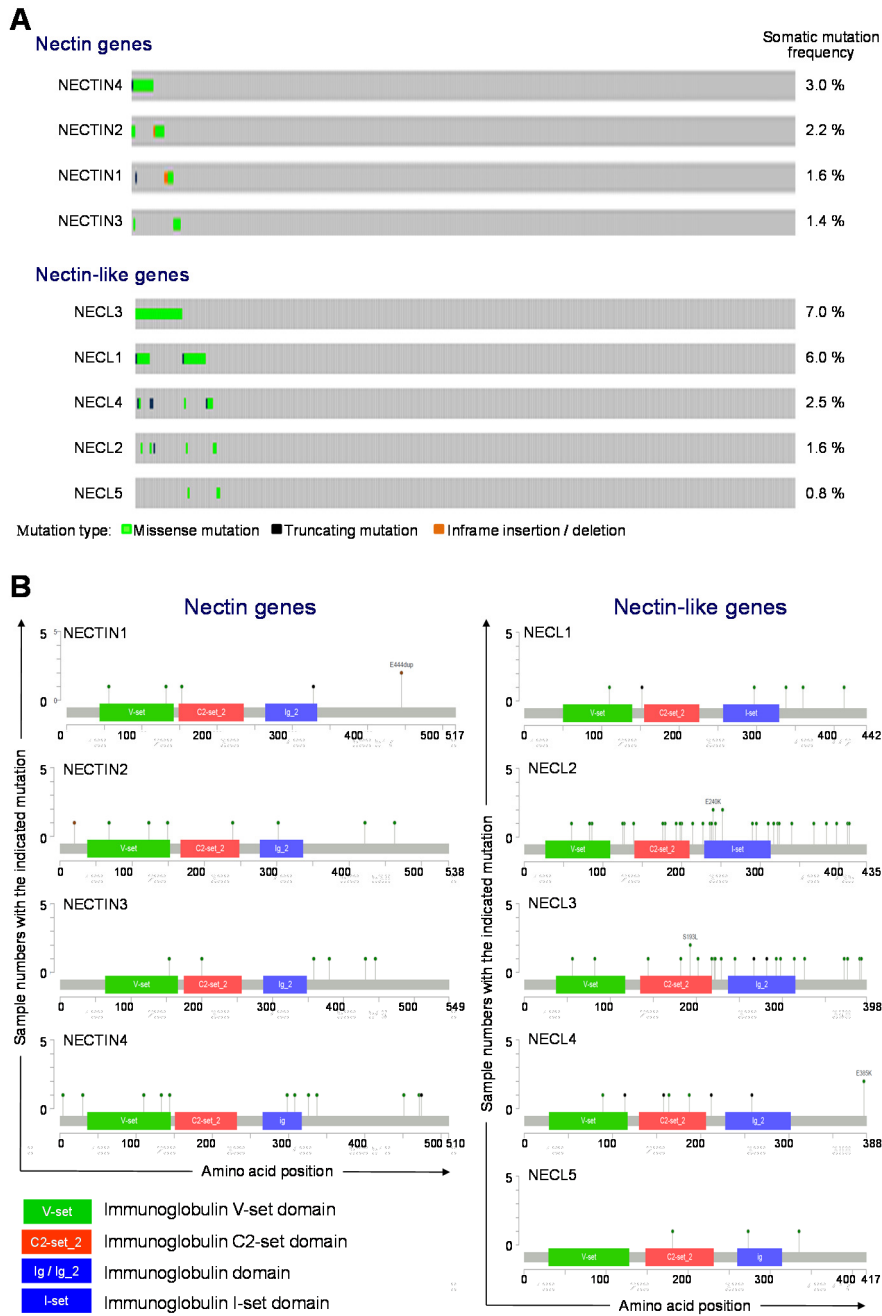
Figure S2. Mutations in nectin and nectin-like genes in skin cutaneous melanoma. (A) Mutation frequencies and (B) mutational profiles of nectin and nectin-like genes in skin cutaneous melanoma were analyzed by using NGS data from the TCGA cohort (TCGA, PanCancer Atlas; n = 448).
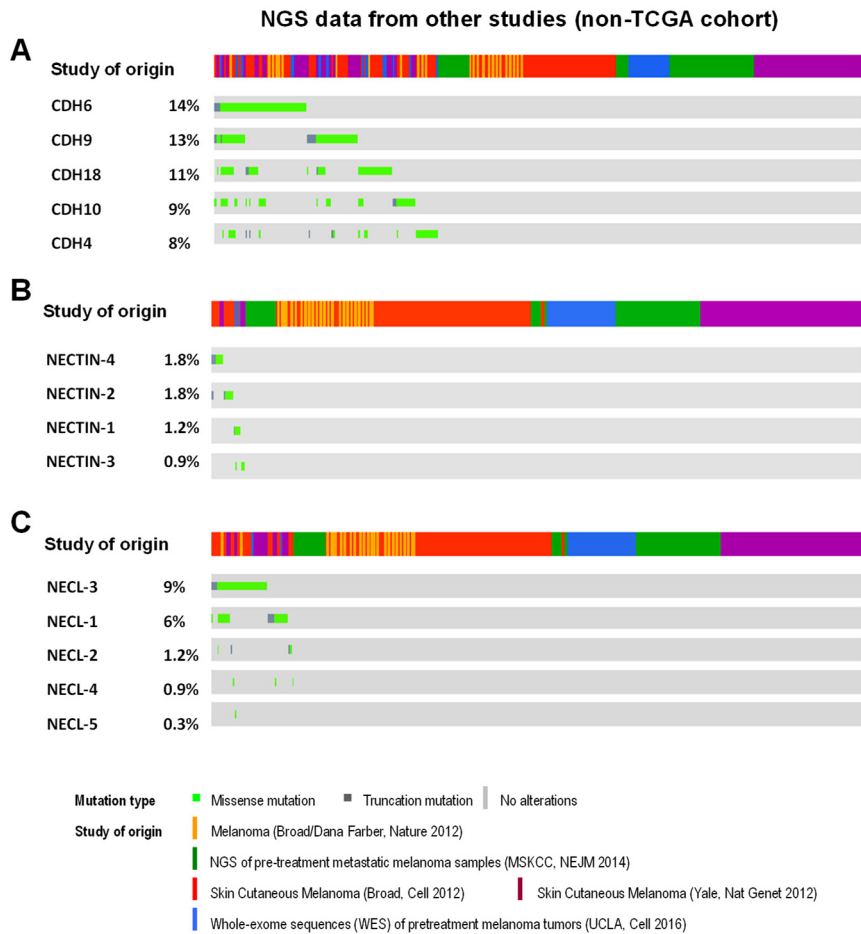
Figure S3. Validation of mutation frequencies in key adherens junction (AJ) genes in non-TCGA cohort. Mutation frequencies of key AJ genes, including (A) top-five highly-mutated cadherin genes identified in TCGA cohort, (B) nectin and (C) nectin-like genes, were analyzed by using NGS data from non-TCGA cohort (n = 396). The non-TCGA cohort include patients from Broad/Dana Farber (n = 26, Nature 2012), MSKCC (n = 64, NEJM 2014), Broad (n = 121, Cell 2012), Yale (n = 147, Nat Genet 2012), and UCLA (n = 38, Cell 2016).

CDH6

melanocyte

Melanoma-WT

Asp **G**AT → **A**AT Asn

Melanoma-D724N

CDH6 · DAPI · β-catenin · merged

Figure S4. Dual-color immunofluorescence staining of CDH6 and β-catenin on melanoma tissues from Taiwanese patients. Tissue sections were prepared from Taiwanese patients with melanoma. Dual-color immunofluorescence staining, red for CDH6 and green for β-catenin, was performed on melanocyte from normal skin epithelium counterpart (*upper*), melanoma with wild type CDHs (*middle*), and melanoma with D724N mutation (*lower*). Cell nuclei were counterstained with DAPI.

CDH9

melanocyte
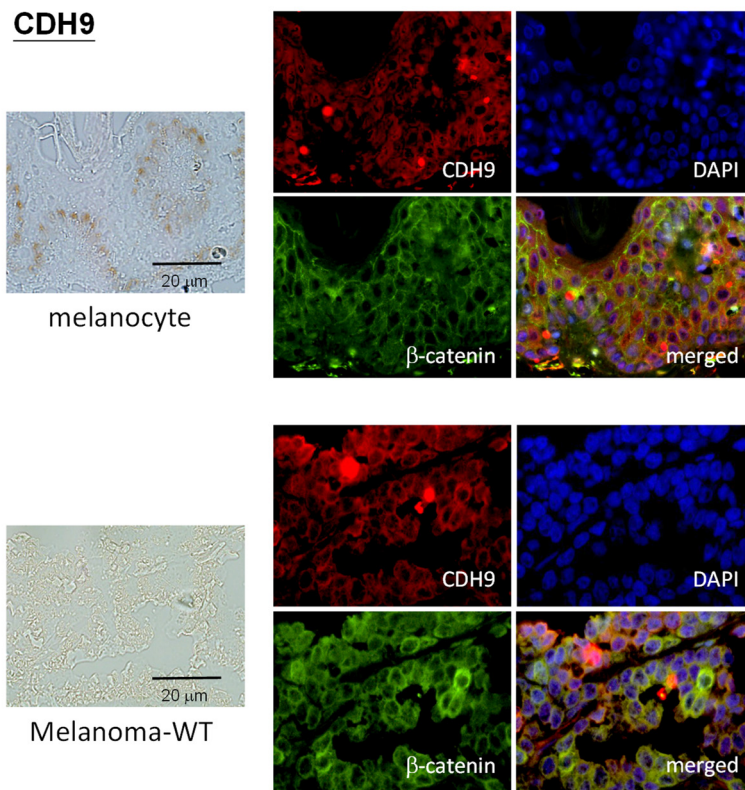
Melanoma-WT

No mutation was detected in the intracellular domain of CDH9 in Taiwanese patients.

Figure S5. Dual-color immunofluorescence staining of CDH9 and β-catenin on melanoma tissues from Taiwanese patients. Tissue sections were prepared from Taiwanese patients with melanoma. Dual-color immunofluorescence staining, red for CDH9 and green for β-catenin, was performed on melanocyte from normal skin epithelium counterpart (*upper*), melanoma with wild type CDHs (*middle*). Cell nuclei were counterstained with DAPI.

CDH10

melanocyte

Melanoma-WT

Glu **G**AG → **A**AG Lys

Melanoma-E682K

CDH10 — DAPI — β-catenin — merged

20 μm
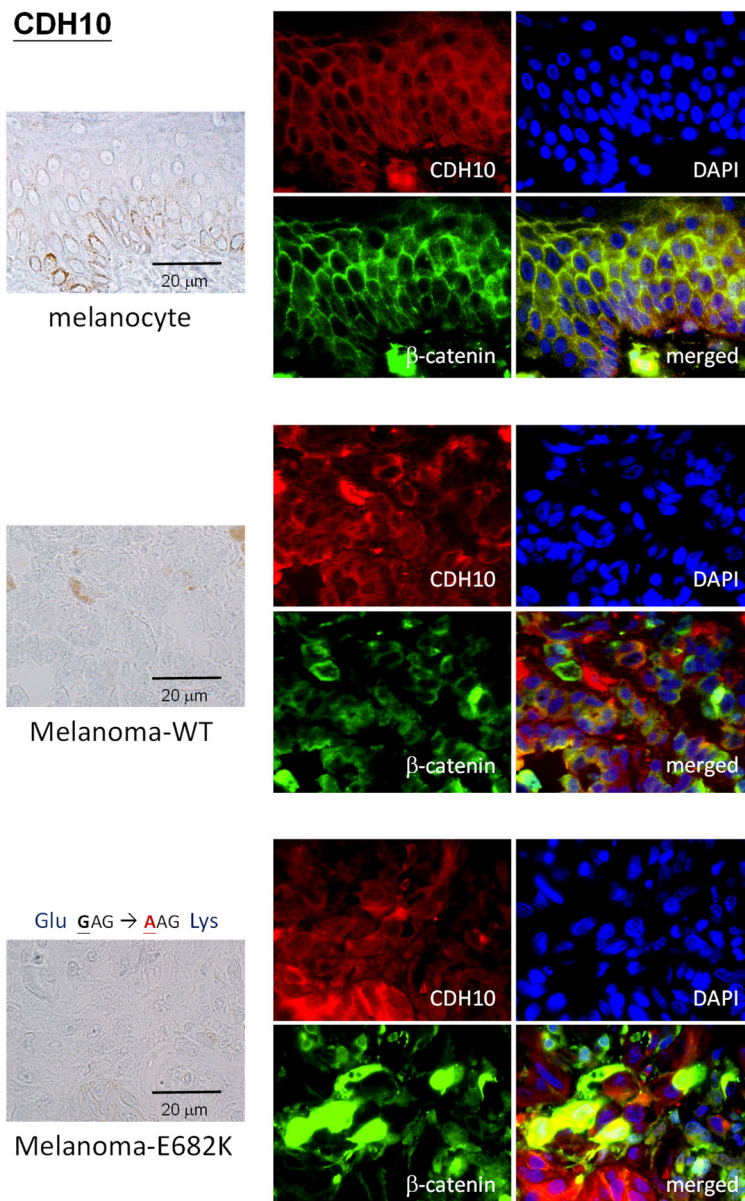
Figure S6. Dual-color immunofluorescence staining of CDH10 and β-catenin on melanoma tissues from Taiwanese patients. Tissue sections were prepared from Taiwanese patients with melanoma. Dual-color immunofluorescence staining, red for CDH10 and green for β-catenin, was performed on melanocyte from normal skin epithelium counterpart (*upper*), melanoma with wild type CDHs (*middle*), and melanoma with E682K mutation (*lower*). Cell nuclei were counterstained with DAPI.
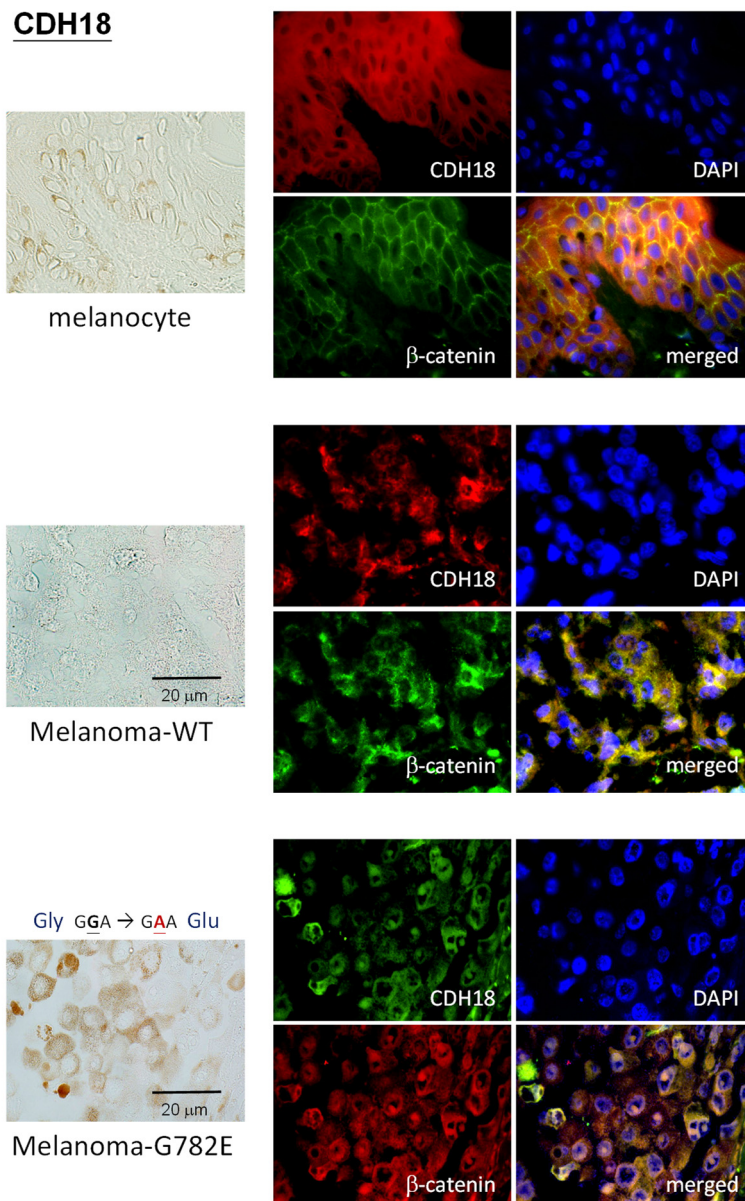
Figure S7. Dual-color immunofluorescence staining of CDH18 and β-catenin on melanoma tissues from Taiwanese patients. Tissue sections were prepared from Taiwanese patients with melanoma. Dual-color immunofluorescence staining, red for CDH18 and green for β-catenin, was performed on melanocyte from normal skin epithelium counterpart (*upper*), melanoma with wild type CDHs (*middle*), and melanoma with G782E mutation (*lower*). Cell nuclei were counterstained with DAPI.
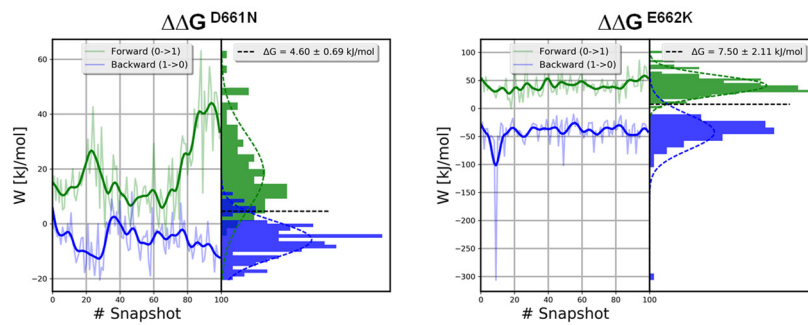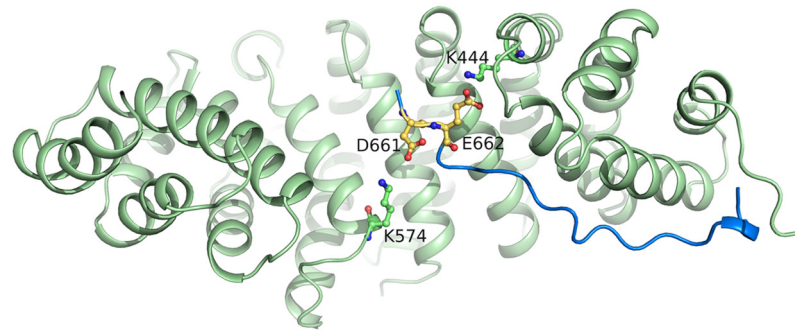
Figure S8. The predicted CDH6/p120-catenin (δ-catenin) complex structures and their binding free energy differences (ΔΔ*G*) between WT and MT CDH6. (A) The predicted structure of JMD (residues 660-677, in blue) in complex with p120-catenin (δ-catenin, in green) was generated by using the MODELLER program. The known mutated sites, D661 and D662, on the JMD (in orange) were found to interact with K444 and K574 on the p120-catenin, respectively. (B) A double-system/single-box setup was used to estimate the binding free energy differences (ΔΔ*G*) caused by mutations.
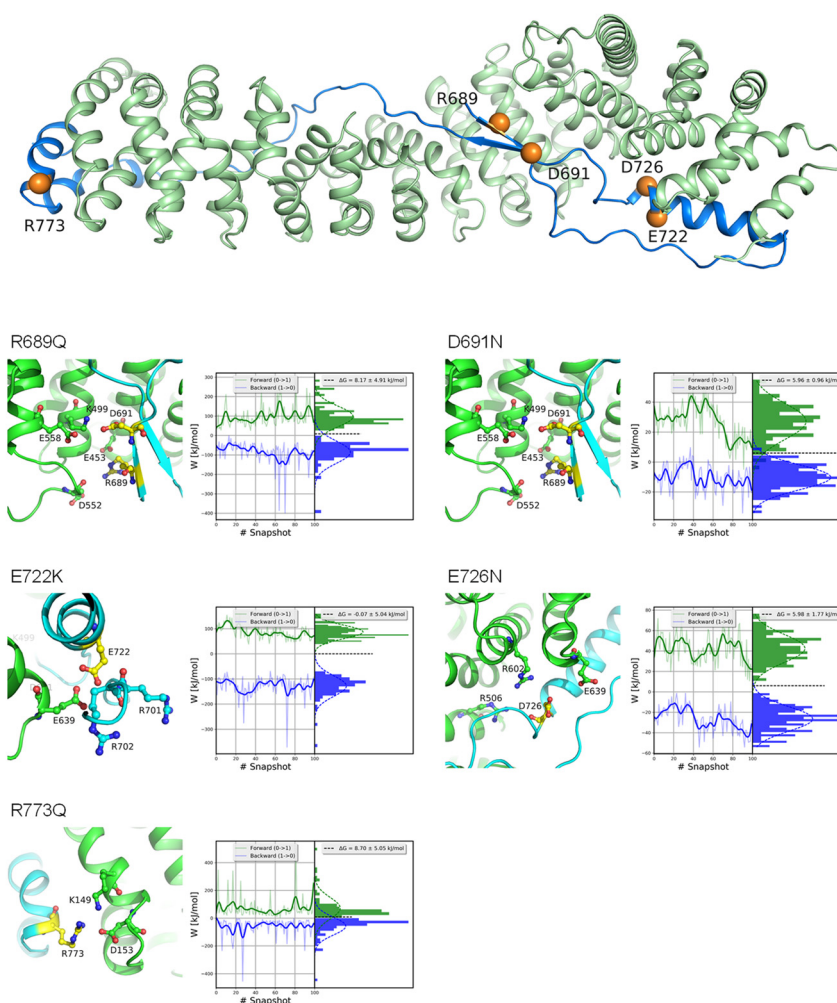
**Figure S9. The predicted CDH6/β-catenin complex structures and their binding free energy differences (ΔΔG) between WT and MT CDH6.** (A) The predicted structure of CBD (residues 687-784, in blue) in complex with β-catenin (green) was generated by using MODELLER program. The known mutated sites were highlighted in orange spheres. A double-system/single-box setup was used to estimate the binding free energy differences (ΔΔG) caused by (B) R689Q, (C) D691N, (D) E722K, (F) E726N, and (G) R773Q substitutions. Cartoon representations indicated the binding interfaces between mutated residues on CBD (yellow) and the interacting residues on β-catenin.
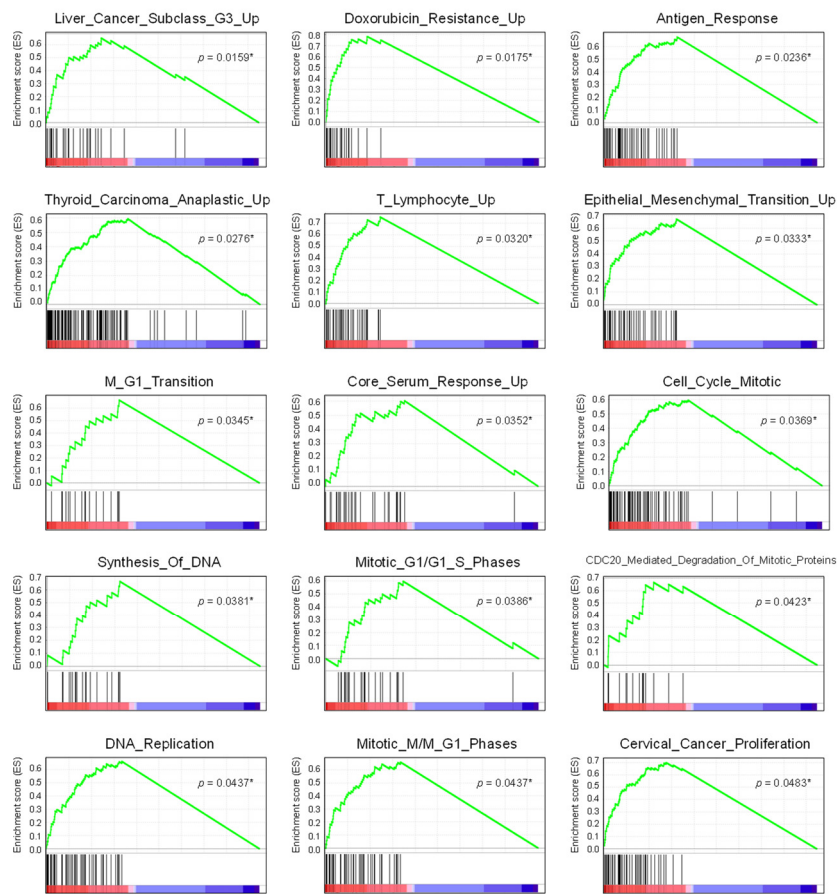
Figure S10. Reactomes/pathways associated with mutations in top-four highly mutated cadherin (core CDHs) genes in skin cutaneous melanoma. Gene set enrichment analysis (GSEA) was performed using mRNA expression data from the TCGA group (TCGA, PanCancer Atlas; n = 448). Patients without mutations in any cadherin genes were utilized as the controls. Concurrent up-regulated reactomes with *p*-values less than 0.05 were shown here. Two pathways, Antigen Response and T-Lymphocyte Up, were also shown in Fig. 7C.
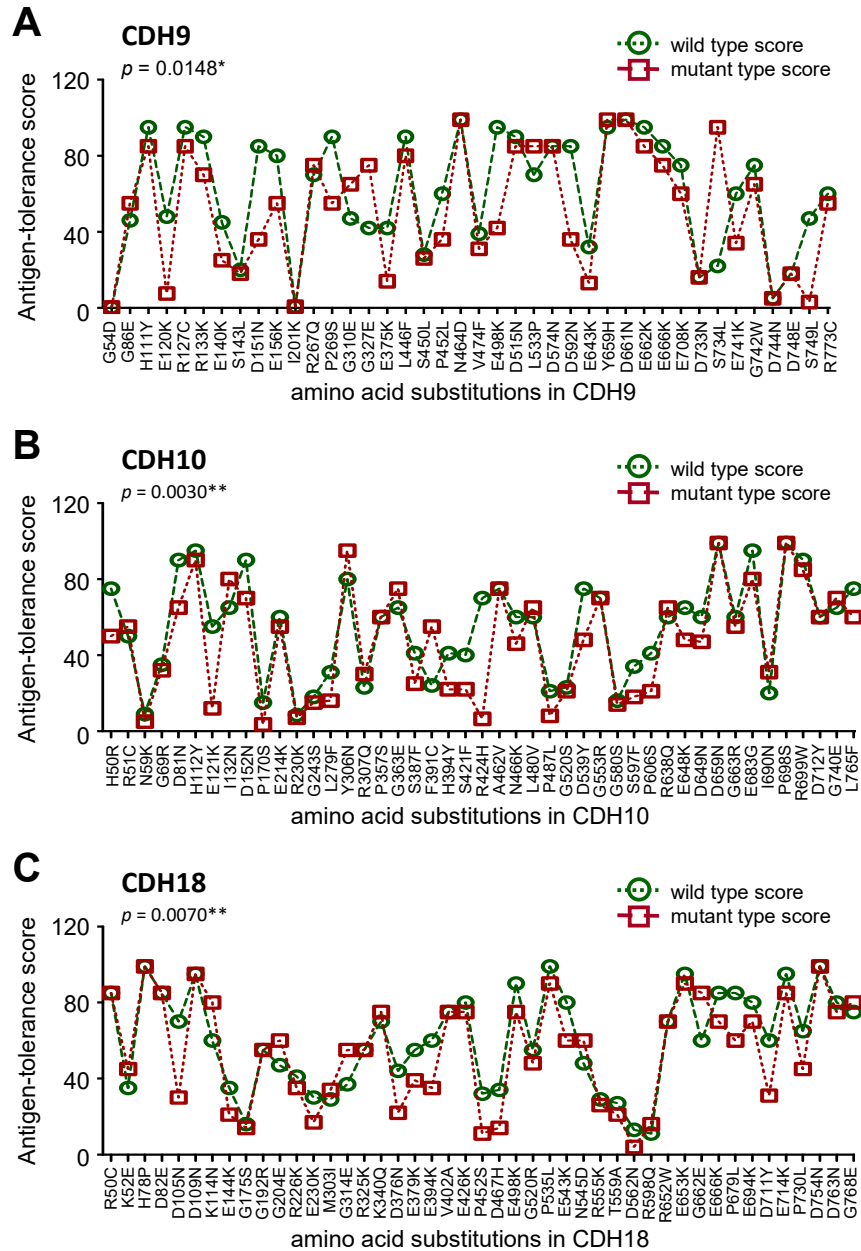
Figure S11. Neo-antigen potentials of mutations in core CDH genes in skin cutaneous melanoma. Antigen-tolerance scores of known mutations in the extracellular domain of (A) CDH9; (B) CDH10; and (C) CDH18 were analyzed by using NetMHCpan algorithm and compared with the scores with wild type sequence. Substitutions with lower scores indicate higher neo-antigen potentials. Two-way ANOVA was utilized to compare the differences between wild type and mutant type. Statistical significance: *, $p < 0.05$; **, $p < 0.01$.
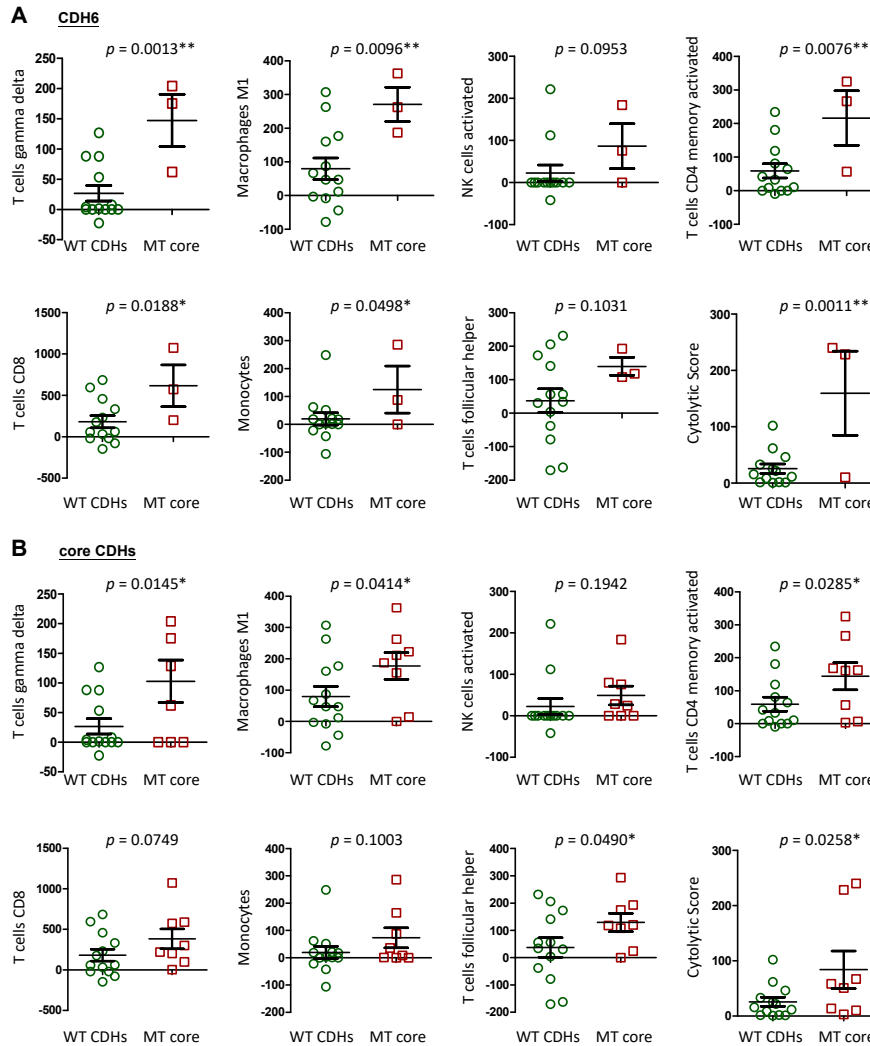
Figure S12. Changes of tumor microenvironments in skin cutaneous melanoma by mutations in core CDH genes. Microenvironment immune types were analyzed in tumors with mutations in (A) *CDH6* or (B) core CDH genes, and compared with the data in tumors with wild type CDHs. The immune scores include γδT cells, M1 macrophages, activated NK cells, activated CD4+ memory T cells, CD8$^+$ T cells, monocytes, follicular helper T cells and cytolytic score.